Available online at www.sciencedirect.com
ScienceDirect
International Journal of Heat and Fluid Flow 28 (2007) 630–637
International Journal of HEAT AND FLUID FLOW
www.elsevier.com/locate/ijhff

The effect of turbulence on the efficiency of the rotational phase separator

J.G.M. Kuerten *, B.P.M. van Esch, H.P. van Kemenade, J.J.H. Brouwers

Department of Mechanical Engineering, Technische Universiteit Eindhoven, P.O. Box 513, NL-5600 MB Eindhoven, The Netherlands

Received 18 October 2006; received in revised form 11 January 2007; accepted 29 March 2007
Available online 11 May 2007

Abstract

The rotational phase separator (RPS) is a device to separate liquid or solid particles from a lighter or heavier fluid by centrifugation in a bundle of channels which rotate around a common axis. Originally, the RPS was designed in such a way that the flow through the channels is laminar in order to avoid eddies in which the particles keep circulating and do not reach the walls. However, in some applications the required volume flow of fluid is so large, that turbulent flow can no longer be avoided. Direct numerical simulation of the flow in a single rotating pipe and particle tracking in this flow are applied to study the influence of turbulence on the collection efficiency of the RPS. The results show that the collection efficiency for larger particles decreases by up to 25% due to the turbulence, whereas the collection efficiency for smaller particles is unaffected. The adverse effect of the resulting swirling flow is partly counteracted by turbulent dispersion. For high rotational speeds the efficiency decreases further as the particles are trapped in a counter-rotating vortex.

Keywords: Phase separation; Turbulence; DNS

1. Introduction

The rotational phase separator (RPS) is a separation technology built around a rotating filter element comprising a multitude of small parallel channels. The filter element can be used in addition to a conventional tangential or axial cyclone to enhance the collection efficiency by one order of magnitude in terms of particle diameter (Brouwers, 2002; Brouwers, 1996; Van Kemenade et al., 2003; Kuerten et al., 2005). Although in practical applications a pre-separator is incorporated to remove coarse particles or droplets, in a conservative design strategy only the separation performance of the filter element itself is considered. Usually, the flow in the channels of the filter element is kept in the laminar regime to prevent capture of particles or droplets in turbulent eddies or swirls. In case of the tangential design (see Fig. 1), mainly used to separate droplets or particles from a gas flow, it is normally not a problem to design within this limit as the throughput is low compared to the flow area of the cyclone and filter element. The filter element is close-coupled with a radial fan at the downstream end. Dynamic pressure is subsequently recovered in the volute type casing around the fan. In typical applications, the main design criterion is the pressure drop over the separator, while the dimensions are of less concern.

The opposite holds for the axial version (Fig. 2) which is mainly used for in-line (offshore) separation of condensed or de-sublimated droplets from another liquid or gas flow. In this design special care is taken in the sizing of the post-separator, where large-size droplets are separated by centrifugation in the swirling flow. The filter element in this case acts as a coalescer (Van Wissen, 2006). In those applications 100% collection of particles is not necessary and the laminar flow condition may impose a too severe restriction on the design. However, in many cases the Reynolds number is low enough for the flow and particle behaviour to be studied in detail by means of direct numerical simulation of the fluid flow and Lagrangian particle tracking. In this

* Corresponding author. Tel.: +31 40 2472362; fax: +31 40 2475399.
E-mail address: j.g.m.kuerten@tue.nl (J.G.M. Kuerten).

0142-727X/$ - see front matter © 2007 Elsevier Inc. All rights reserved.
doi:10.1016/j.ijheatfluidflow.2007.03.003

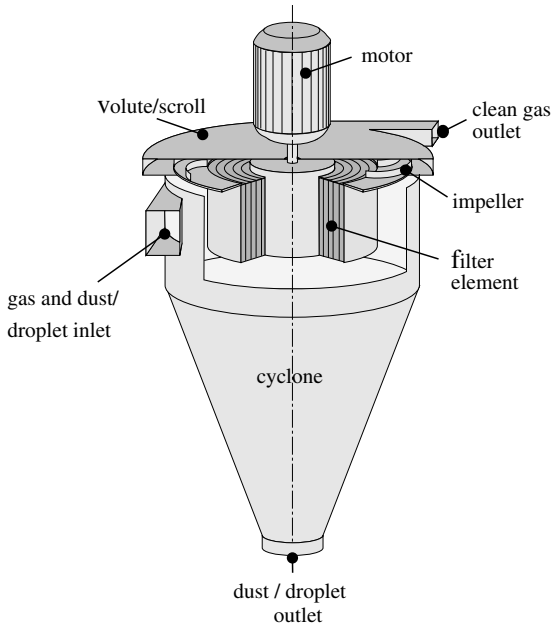

Fig. 1. RPS mounted in a cyclone in the tangential version.

study, the consequences of allowing low turbulent conditions in the channels of the filter element are investigated by comparing the results of an analytical model for the laminar regime with turbulent DNS results. Since this study is performed for the case that the channels of the filter element are circular, we will use the term pipe for a channel in the following.

In Section 2 of this paper the analytical model for the calculation of particle collection efficiency will be presented. Section 3 provides the governing equations and numerical method for the DNS of particle-laden flow in a rotating pipe and in Section 4 results are presented. Finally, in Section 5 the conclusions of the paper and an outlook to future work are given.

2. Analytical model

Brouwers (1997) derived the elementary particle collection efficiency of the rotational phase separator for channels with circular, triangular and sinusoidal shape in case the flow in the channels is laminar. At entry of the filter element, or soon after, the fluid co-rotates with the filter element. As we are concerned with particles (or droplets) in the micrometer range, inertial forces are neglected (Hinds, 1982). Whether a particle reaches the outer wall depends on the distance to be traveled by the particle, the centrifugal force, the axial velocity profile and the length of the pipe. The centrifugal force depends on the angular velocity of rotation, the difference in mass density between particle and fluid, the particle diameter and the distance between particle and axis of rotation. The velocity at which the particles move radially can be calculated using Stokes' law for drag force. Assuming a constant axial fluid velocity U_b and a uniform distribution of the particles over the cross-sectional area, an expression can be derived for $d_{p,100}$, the diameter of the smallest particle which is collected with 100% probability in a pipe at a radial location R (Brouwers, 1997):

$$d_{p,100}^2 = \frac{18\mu U_b D}{(\rho_p - \rho_f)\Omega^2 RL}. \quad (1)$$

Here μ denotes the dynamic viscosity of the fluid, D the pipe diameter, ρ_p and ρ_f the mass density of the particle and fluid, Ω the angular velocity and L the length of the pipe.

Moving with the gas through the pipe, all particles of a certain diameter will move with the same velocity in the radial direction. If a collection wall were absent, at the exit of the pipe two cross-sectional areas could be distinguished (see Fig. 3): the cross-sectional area of the pipe itself and the cross-sectional area formed by the particles. The ratio of particles that do not reach the wall to the total number of particles is equal to the ratio of the shaded area to the total cross-section of the pipe.

To derive an expression for the particle collection efficiency in the presence of a Hagen–Poiseuille velocity

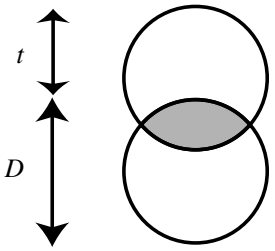

Fig. 3. Centrifugally induced particle displacement in a pipe.

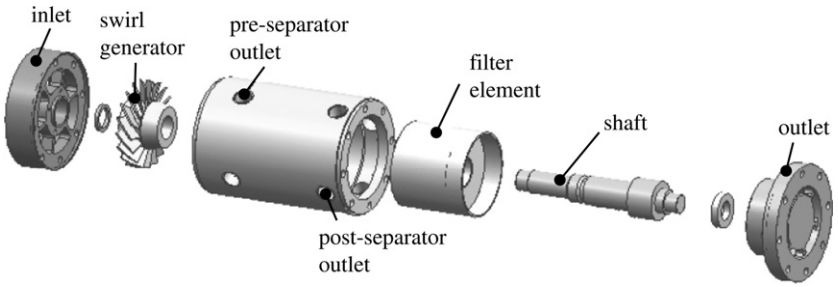

Fig. 2. Axial version of RPS in an inline configuration, separating liquid droplets from a gas.

profile, the circular cross section is divided into a system of parallel planes within which the movement of particles takes place. Eq. (1) can be used for the local conditions. Subsequent integration gives the particle collection efficiency η in one pipe subject to Hagen–Poiseuille flow

$$\eta = \begin{cases} \frac{4}{\pi}x^2 a - \frac{4}{3\pi}\sqrt{(1-a^2)}a\left(\frac{5}{2}-a^2\right) - \frac{2}{\pi}\arcsin(a) + 1 \\ \quad \text{if } x < \sqrt{4/3} \\ 1 \quad \text{if } x \geqslant \sqrt{4/3}. \end{cases} \tag{2}$$

Here $a = [1-(3x^2/4)^{2/3}]^{1/2}$ and the dimensionless particle diameter $x = d_p/d_{p,100}$. Using the same procedure also expressions for channels with a sinusoidal and with a triangular shape are derived. Note that the efficiency of a channel depends on its radius R within the filter element and the local axial fluid velocity. The efficiency of the total filter element can be calculated from the efficiency of a single channel by integrating over the cross-sectional area and taking into account non-uniform axial fluid velocity and particle density. The collection efficiency of a single channel is given in Fig. 4. Included are experimental results of collection efficiency for complete separation devices which consist of an RPS mounted on a cyclone or swirl generator and for which the flow in the channels of the RPS is laminar (Brouwers, 2002; Mondt et al., 2004; Mondt et al., 2006). In all applications the RPS was designed based on the separation efficiency of the filter element alone. The figure shows that the theoretical collection efficiency of a single channel is a conservative indication of the practical collection efficiency of a complete device. The observation that the experimentally obtained collection efficiency is larger than the theoretical value can be explained by the collection properties of the pre-separator.

In this study the case of a circular geometry is adopted, as there are more reference cases available (Schlichting, 1979; Brouwers, 1995) and a DNS is more easily feasible.

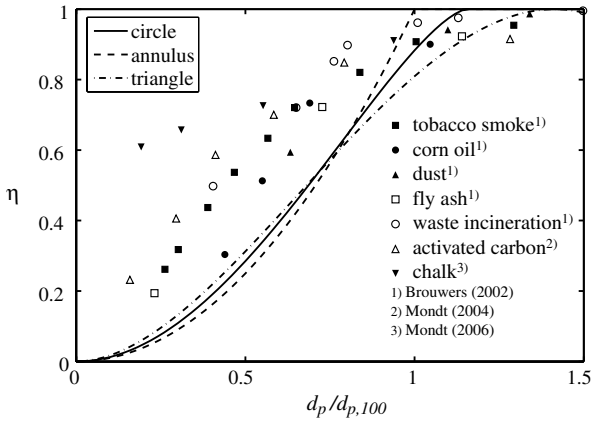

Fig. 4. Collection efficiency of one channel of an RPS in laminar conditions for various channel shapes. Also included are experimental results.

3. Numerical method

In the DNS the three-dimensional Navier–Stokes equation for incompressible flow is solved in a cylindrical geometry in the vorticity formulation. The equation is solved in a rotating frame of reference and reads:

$$\frac{\partial \vec{u}}{\partial t} + \vec{\omega}\times\vec{u} + \vec{\Omega}\times\vec{\Omega}\times\vec{r} + 2\vec{\Omega}\times\vec{u} = -\frac{1}{\rho}\nabla P + \nu\Delta\vec{u}. \tag{3}$$

Here P denotes the total pressure, $P = p + \frac{1}{2}\rho u^2$, $\vec{u}$ the fluid velocity, $\vec{\omega}$ the fluid vorticity, ρ the fluid density, ν the kinematic viscosity and $\vec{r}$ the position vector with respect to the rotation axis. Compared to the Navier–Stokes equation in a stationary frame of reference, two additional terms appear. The centrifugal force, $\vec{\Omega}\times\vec{\Omega}\times\vec{r}$, can be incorporated in the pressure (Brouwers, 2002). The Coriolis force, $2\vec{\Omega}\times\vec{u}$, does not depend on the distance to the rotation axis. Hence, the fluid velocity does not depend on this distance, which implies that in one DNS calculation the flow in all pipes in the bundle can be simulated. Note however, that the pressure field does depend on this distance; only the sum of the pressure and centrifugal pressure is independent of the distance to the rotation axis.

In the analysis only fully-developed pipe flow is considered. The entrance length in which the developed pipe flow is established is omitted. For the Reynolds numbers considered here, the entrance length is on the order of $5D$, which is a small fraction of the typical length of the pipe. The design of the filter element compensates for this entrance length as a conservative approach. In the DNS a pipe of a finite length equal to five times its diameter is taken with periodic boundary conditions in the axial direction. Since the tangential direction is periodic by definition, a spectral method with a Fourier–Galerkin approach in the two periodic directions is a natural choice. In the radial direction a Chebyshev-collocation method is applied, but, in order to avoid a large number of collocation points near the axis of the pipe, the radial direction is divided into five elements with a Chebyshev grid in each element (Walpot et al., 2006). The coupling between the elements is continuously differentiable. The choice for five elements is a compromise between collocation point distribution and accuracy. More elements can lead to a better distribution of collocation points, but, since the continuity conditions are imposed at the element boundaries instead of the Navier–Stokes equation, this results in a decrease in accuracy.

For integration in time a second-order accurate time-splitting method is chosen. In the first step the nonlinear terms, including the Coriolis force, are treated in an explicit way. The nonlinear terms are calculated pseudo-spectrally by fast Fourier transform, where the 3/2-rule is applied to prevent aliasing errors. In the second step the pressure is calculated in such a way that the velocity field at the new time level is approximately divergence free. Finally, in the last step the viscous terms are treated implicitly. Since the Fourier modes can be completely decoupled, only a one-dimensional system of equations needs to be solved

for each Fourier mode. The wall of the pipe acts as a no-slip wall. The wall boundary condition for the pressure follows from the wall-normal component of the Navier–Stokes equation, whereas the correct boundary conditions at the pipe axis follow from the property that the Cartesian velocity components and pressure are single-valued and continuously differentiable there.

The mean axial pressure gradient is chosen in such a way that the volume flow, and hence the Reynolds number based on the bulk velocity, remains constant. The simulations are started from an arbitrary initial solution. After a large number of time steps a state of statistically stationary turbulent flow is reached. In Walpot et al. (2006) it is shown that for turbulent flow in a non-rotating pipe the DNS results for mean flow, velocity fluctuations and terms in the kinetic energy balance agree well with results of other DNS codes (Veenman, 2004; Loulou, 1996; Wagner et al., 2001) and experimental results (Westerweel et al., 1996).

Particle-laden flows can be described in two different ways. In Lagrangian methods an equation of motion for each particle is solved, whereas in Eulerian methods the particles are described as a second phase for which conservation equations are solved. Lagrangian methods (Yeung and Pope, 1988) are useful if the number of particles is not too large. Forces exerted by the fluid on the particles can easily be incorporated and for low particle mass loadings the effect of the particles on the fluid and the effect of interactions between particles are negligible. Eulerian methods (Markatos, 1986) are necessary if the number of particles is large.

We have chosen for a Lagrangian approach for two reasons. First, the number of particles is limited and the particle mass loading small, so that a Lagrangian method with one-way coupling is possible. Second, the length of an actual pipe of an RPS is much larger than the length of the pipe used in the DNS. In Eulerian approaches a particle concentration field for the whole pipe length and for each particle diameter would be needed, which leads to huge memory and computational requirements. Hence, particles are tracked by solving an equation of motion for each particle. If $\vec{x}$ is particle position and $\vec{v} = \mathrm{d}\vec{x}/\mathrm{d}t$ its velocity, the equation of motion reads in general:

$$m\frac{\mathrm{d}\vec{v}}{\mathrm{d}t} = \sum \vec{f}. \tag{4}$$

Here m denotes the mass of the particle and the right-hand side contains all forces acting on the particle. In the simulations considered here, we restrict to cases where particles are small and have a large mass density compared to the fluid mass density. As a result the only forces which cannot be neglected are the drag force and centrifugal force. This leads to an equation of motion of the form (Maxey and Riley, 1983):

$$\frac{\mathrm{d}\vec{v}}{\mathrm{d}t} = \frac{\vec{u}(\vec{x},t) - \vec{v}}{\tau_\mathrm{p}}\left(1 + 0.15Re_\mathrm{p}^{0.687}\right) + \Omega^2(R\vec{e}_x + \vec{r}_2), \tag{5}$$

where τ_p is the particle relaxation time, $\vec{e}_x$ is the unit vector in the direction from the rotation axis to the pipe axis and $\vec{r}_2$ the position vector of the particle in the two-dimensional plane perpendicular to the pipe axis. The standard drag correlation for particle Reynolds number, $Re_\mathrm{p} = d_\mathrm{p}|\vec{u} - \vec{v}|/\nu$, between 0 and 1000 is used (Clift et al., 1978). Note that in contrast to the fluid velocity, the particle equation of motion depends on the distance between the pipe axis and axis of rotation through the centrifugal force. Since the particle relaxation times of the particles considered are very small, the inertia term in Eq. (5) could be neglected. However, since the equation is nonlinear in the particle velocity, it is easier to solve it in this way. A partially implicit two-step Runge–Kutta method is used to this end. Finally, the fluid velocity at the particle position, which appears in Eq. (5) is found by fourth-order accurate interpolation from its values at grid points.

The particle simulations start from a fully-developed turbulent velocity field with a homogeneous distribution of particles over the entire pipe. The initial particle velocity is chosen in such a way that its initial acceleration equals zero. In a real RPS the length of a pipe is much larger than the length of the computational domain. Therefore, if a particle reaches the end of the computational domain in the axial direction, it is re-inserted at the corresponding position at the pipe entrance until it has traveled an axial distance equal to the length of the real pipe. If a particle reaches the wall of the pipe before it travels the whole length it is considered as being collected. Indeed, the centrifugal velocity of the small particles under consideration is so small (less than 1 cm/s), that almost all particles will stick to the wall, or to the layer of particles already present there.

In an actual experiment where the particles are homogeneously distributed over the total flow domain, the number of particles that enter a pipe of the RPS at a certain radial position, is proportional to the axial velocity at that position. Therefore, in the calculation of the collection efficiency, each particle has a weight proportional to its initial axial velocity.

The computer program has been implemented on a linux cluster of PC's, where it is parallelized with the use of MPI. A full simulation of fluid and 400,000 particles takes two weeks on 8 processors.

4. Results

In this section results will be presented. We will consider only one test case. Results of other simulations will be presented elsewhere. The fluid flow is determined by two non-dimensional parameters, the bulk Reynolds number $Re = U_\mathrm{b}D/\nu$ and the rotation Reynolds number $Re_\Omega = \Omega D^2/4\nu$, where U_b is the bulk velocity and D the diameter of the pipe. In the test case considered $Re = 5300$ and $Re_\Omega = 980$. The ratio of the rotation Reynolds number and the bulk Reynolds number is related to the rotation number used by Orlandi and Fatica (1997). The rotation

number in our simulations equals 0.37. The DNS is performed with 106 collocation points in the wall-normal direction and 128 Fourier modes in both the axial and tangential direction.

In the following, results of the fluid calculations will be presented and analyzed first, and then the results of the particle simulations will be discussed.

4.1. Fluid properties

In flow in a non-rotating pipe, time-averaged quantities depend on the radial coordinate only and the mean radial and tangential velocity components are equal to zero. This follows from the axial symmetry of the problem and the continuity equation. For rotating pipe flow, this symmetry is partly broken. Time-averaged quantities still depend on the radial coordinate only and from the continuity equation it still follows that the mean radial velocity component equals zero, but the mean tangential velocity is no longer equal to zero.

A second difference between flow in a non-rotating and in a rotating pipe is the region where the laminar Poiseuille flow becomes unstable. It is well known that linear stability theory predicts that Poiseuille flow in a non-rotating pipe is stable at all Reynolds numbers. Transition to turbulence occurs through the nonlinear interaction of perturbations of finite amplitude. However, it has been shown that already a small rotation rate leads to linear instability (Mackrodt, 1976; Fernandez-Feria and Del Pino, 2002; Sanmiguel-Rojas and Fernandez-Feria, 2005). The flow case we consider in this paper is at a bulk Reynolds number for which the flow without rotating wall is also turbulent. In Fig. 5 the mean tangential velocity component in wall units is plotted as a function of the radial coordinate. In this figure also the result for the same bulk Reynolds number and $Re_\Omega = 490$ is included. It can be seen that the mean tangential velocity is almost exactly linearly dependent on Re_Ω when scaled with the friction velocity,

$$u_\tau = \sqrt{\nu \left.\frac{\mathrm{d}\bar{u}_z}{\mathrm{d}r}\right|_{r=D/2}} \tag{6}$$

The non-zero mean tangential velocity can be understood from the equation for the radial-tangential component of the Reynolds stress tensor, which reads after disregard of the very small viscous terms:

$$\begin{aligned}\bar{u}_\phi\left(2\overline{u_\phi'^2} - \overline{u_r'^2}\right) - r\overline{u_r'^2}\frac{\mathrm{d}\bar{u}_\phi}{\mathrm{d}r} &= -2\Omega r\left(\overline{u_\phi'^2} - \overline{u_r'^2}\right) + \frac{1}{r}\frac{\mathrm{d}}{\mathrm{d}r}\left(r^2\overline{u_r'^2u_\phi'}\right) - \overline{u_\phi'^3} \\ &\quad + \frac{1}{\rho}\left(r\overline{u_\phi'\frac{\partial p'}{\partial r}} + \overline{u_r'\frac{\partial p'}{\partial \phi}}\right).\end{aligned} \tag{7}$$

In this expression primes denote the fluctuating part of a quantity, subscripts r and ϕ refer to the radial and tangential component and bars denote mean quantities. The third order moments appearing in Eq. (7) turn out to be very small throughout the pipe, whereas the last term on the right-hand side is only significant close to the wall of the pipe. Furthermore, due to the behaviour of the tangential velocity component near the pipe axis $r\mathrm{d}\bar{u}_\phi/\mathrm{d}r \cong \bar{u}_\phi$ there. Therefore, Eq. (7) simplifies to $\bar{u}_\phi \cong -\Omega r$ close to the axis of the pipe. The results presented in Fig. 5 indeed agree with this behaviour close to the axis of the pipe.

A further fluid property which is important for the understanding of particle behaviour is the fluctuating part of the fluid velocity in the plane perpendicular to the pipe axis. In Fig. 6 the root-mean-square of the tangential velocity component is plotted as a function of the radial coordinate in wall units. Included are results at $Re_\Omega = 490$ and in a non-rotating pipe. It can be seen that the rotation slightly increases the velocity fluctuations and this holds for all three velocity components. Moreover, it appears that the magnitude of the velocity fluctuations is almost equal to the maximum of the mean tangential velocity component in case $Re_\Omega = 980$.

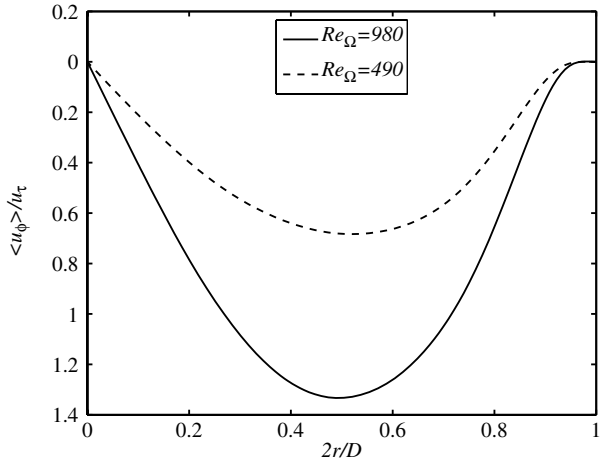

Fig. 5. Mean tangential velocity component in wall units. The brackets have the same meaning as the overbar in the text.

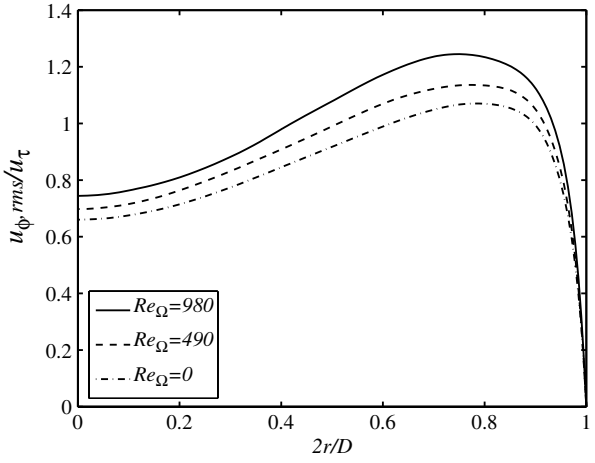

Fig. 6. Root-mean-square of tangential velocity component in wall units.

4.2. Particle behaviour

Particle behaviour in turbulent rotating pipe flow can be understood from a simplified equation of motion in the plane perpendicular to the pipe axis. To this end all forces on the particle are disregarded except the linearized drag force and the centrifugal force. If r and ϕ are the radial and tangential coordinate of a particle, the equations of motion are:

$$\begin{cases} \frac{\mathrm{d}r}{\mathrm{d}t} = u'_r + \tau_\mathrm{p}\Omega^2(r + R\cos(\phi)) \\ r\frac{\mathrm{d}\phi}{\mathrm{d}t} = \bar{u}_\phi + u'_\phi - \tau_\mathrm{p}\Omega^2 R\sin(\phi) \end{cases} \tag{8}$$

The equations of motion contain three different terms: the mean tangential fluid velocity, which has Ωr as order of magnitude, the fluctuating velocity with the friction velocity u_τ as order of magnitude and the last terms on the right-hand side of Eq. (8), which represents the centrifugal velocity. For particles which are just separated in uniform laminar flow, the order of magnitude of the centrifugal velocity equals $U_\mathrm{b}D/L$ with L the length of the pipe. For situations relevant in practice, the centrifugal velocity is always smaller than the fluctuating velocity. In our example calculation the mean tangential velocity is only slightly smaller than the fluctuating velocity.

Before turning to the simulation results, we first consider a calculation of a hypothetical velocity field in which the mean tangential velocity is present, but the velocity fluctuations equal zero. Note that this is not a laminar solution of the Navier–Stokes equation; it only serves to understand the nature of the different contributions to Eq. (8). In Fig. 7 the collection efficiency for this hypothetical flow is compared with the collection efficiency for laminar Hagen–Poiseuille flow. The particle diameter is non-dimensionalized with the smallest diameter which is collected with 100% probability for uniform laminar flow. Fig. 7 shows that the collection efficiency is reduced dramatically by the presence of the axial vortex. Particles are trapped in this vortex and follow a path which differs only slightly from the path they would follow without centrifugal force. Only those particles which are initially close to the wall are collected. This situation is similar to the one obtained for laminar flow in a slightly tilted rotating pipe, which was studied by Brouwers (1995). Also in that case particles are trapped in the secondary flow perpendicular to the pipe axis, which results in a reduced collection efficiency.

Next, we return to particle behaviour in turbulent rotating pipe flow. In the simulation particles with diameters ranging between $0.1d_{\mathrm{p},100}$ and $1.6d_{\mathrm{p},100}$ are inserted in the flow, where $d_{\mathrm{p},100}$ is the smallest particle collected with 100% probability in a uniform laminar flow. For each diameter 25,000 particles are initially uniformly distributed over the pipe and their motion is subsequently tracked by solving their equation of motion until they either reach the wall of the pipe or travel over an axial distance larger than the length of the pipe, which equals $133.5D$. The mass density of the particles equals 22.5 times the mass density of the fluid and only one pipe is considered with its axis at a distance of $26.7D$ from the rotation axis.

In Fig. 8 the collection efficiency calculated in this simulation is compared with the result for a laminar Hagen–Poiseuille fluid velocity profile. Although the collection efficiency for a turbulent RPS is lower than for a laminar RPS, the reduction obtained is not as dramatic as for the hypothetical flow without turbulent velocity fluctuations shown in Fig. 7. Fig. 8 shows that the collection efficiency of the smallest particles is hardly affected by turbulence, whereas the reduction in efficiency for particles near $d_{\mathrm{p},100}$ is almost 30%.

This result can be explained in the following way. First we will consider the largest particles which are separated with 100% probability in a flow with the same mean axial velocity profile as in the turbulent flow, but without velocity fluctuations and mean swirl. In turbulent flow conditions the path of such a particle becomes more irregular due to turbulent velocity fluctuations. The turbulent dispersion of particles at the end of the pipe depends on the magnitude of the velocity fluctuations and the time of travel and is for such a particle on the order of the diameter of the pipe. Hence, due to turbulent velocity fluctuations some

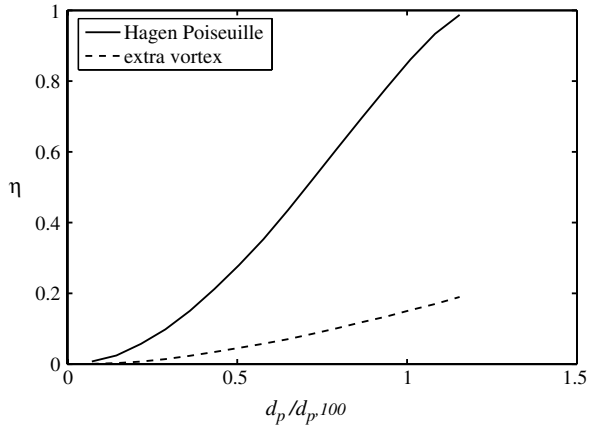

Fig. 7. Collection efficiency for laminar flow with and without extra tangential velocity.

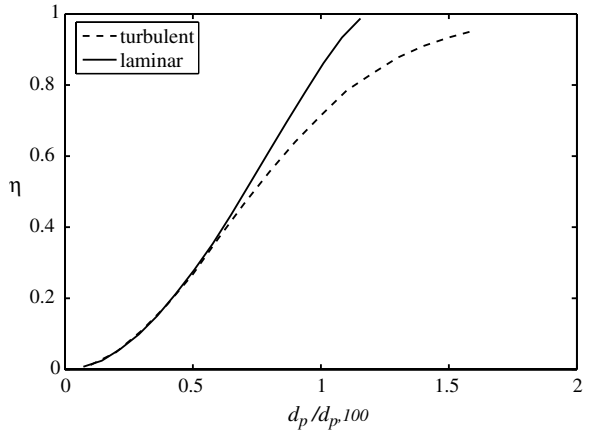

Fig. 8. Collection efficiency for laminar and turbulent flow.

of these particles will reach the collection wall at a more upstream axial position and will still be collected in turbulent flow, whereas other particles would reach the collection wall at a more downstream position and will not be collected in turbulent flow. Hence, the collection efficiency of these particles will decrease in turbulent flow.

On the other hand, some of the particles with a diameter much smaller that are collected in laminar flow conditions, will not be collected in turbulent flow, whereas some of these small particles that are not collected in laminar flow, will be collected due to turbulent velocity fluctuations in turbulent flow. The effects of both phenomena on the total collection efficiency approximately cancel, so that the collection efficiency for small particles is approximately the same in laminar and turbulent flow.

Another conclusion that can be drawn from the simulation results is that $d_{p,100}$ cannot be defined for turbulent flow conditions. Even for large particle diameters, some particles will be trapped in flow structures and will not reach the collecting wall before the end of the pipe.

The results shown in Figs. 7 and 8 imply that the presence of turbulent velocity fluctuations counteracts the trapping of particles in the axial vortex. This is due to the fact that the tangential velocity fluctuations are as large as or larger than the mean tangential velocity. Two extra simulations have been performed to verify this. In the first the Coriolis force in the Navier–Stokes equation has been switched off, but the centrifugal force in the particle equation of motion has been kept. Hence, in this simulation the mean tangential fluid velocity in Eq. (8) equals zero, but the velocity fluctuations are almost the same. The resulting collection efficiency is only slightly higher than the turbulent result in Fig. 8. On the other hand, a simulation with an artificially increased mean tangential velocity by a factor of 3 resulted in a substantial reduction in collection efficiency. The collection efficiency obtained from these two simulations are compared with the results of the ordinary simulation in Fig. 9.

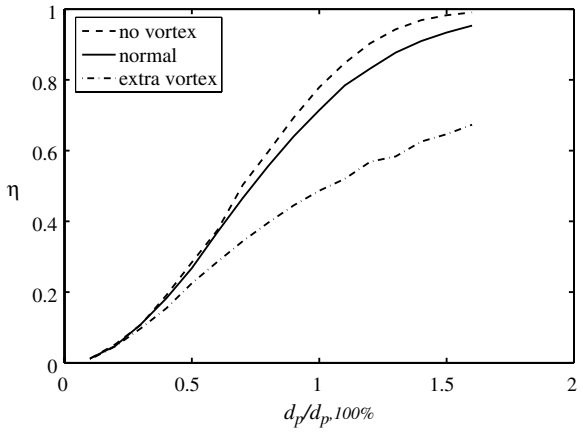

Fig. 9. Collection efficiency for turbulent flow, turbulent flow without vortex and turbulent flow with increased vortex strength.

5. Conclusions and future work

In this paper we studied the effect of turbulent flow in the circular channels of a rotational phase separator on the collection efficiency. To that end direct numerical simulation of the flow and Lagrangian particle tracking were performed. The results of the fluid flow show that an axial vortex is present in the flow, caused by the rotation, but, in contrast to the secondary flow in laminar flow in a slightly tilted pipe, this vortex hardly influences the collection efficiency for the parameter setting of the simulated test case. However, turbulent velocity fluctuations have a negative influence on the collection efficiency, especially for larger particles. One of the consequences is that $d_{p,100}$, the diameter of the smallest particles which is collected with 100% probability, can no longer be defined for turbulent flow conditions. In order to meet design criteria in practice, the length of the RPS should be chosen about 20% larger than laminar design criteria prescribe to obtain the same collection efficiency. The results confirm that when the rotational particle separator is used as a bulk separator and a strictly defined cut-off diameter is not required, the working range can be extended in the turbulent range to enhance the throughput within the same volume constraints. This is a major advantage in offshore applications where platform space and load capacity are at premium and recent designs of the RPS for natural gas treatment (Mondt et al., 2006; Van Wissen, 2006) are operating in the turbulent regime.

In the near future also other test cases will be performed. For other conditions, where particles and particle relaxation times are larger, inertial terms in the particle equation of motion will play a larger role. This implies that the results are also affected by turbophoresis (Kuerten and Vreman, 2005; Reeks, 1983), which drives particles towards the walls of a pipe. Moreover, the effect of turbulent flow in slightly tilted pipes will be studied.

Acknowledgements

This work was sponsored by the National Computing Facilities Foundation, NCF for the use of supercomputer facilities, with financial support from the Netherlands Organization for Scientific Research, NWO.

References

Brouwers, J.J.H., 1995. Secondary flows and particle centrifugation in slightly tilted rotating pipes. Appl. Scientific Res. 55, 95–105.

Brouwers, J.J.H., 1996. Rotational particle separator: a new technology for separating fine particles and mists from gases. Chem. Eng. Technol. 19, 1–10.

Brouwers, J.J.H., 1997. Particle collection efficiency of the rotational particle separator. Powder Technol. 92, 89–99.

Brouwers, J.J.H., 2002. Phase separation in centrifugal fields with emphasis on the rotational particle separator. Exp. Therm. Fluid Sci. 26, 325–334.

Clift, R., Grace, J.R., Weber, M.E., 1978. Bubbles, Drops and Particles. Academic Press.

Fernandez-Feria, R., Del Pino, C., 2002. The onset of absolute instability of rotating Hagen–Poiseuille flow: a spatial stability analysis. Phys. Fluids 14, 3087–3097.

Hinds, W.C., 1982. Aerosol Technology. John Wiley.

Kuerten, J.G.M., Vreman, A.W., 2005. Can turbophoresis be predicted by large-eddy simulation. Phys. Fluids 17, 011701.

Kuerten, J.G.M., Van Kemenade, H.P., Brouwers, J.J.H., 2005. Numerical study of the rotational particle separator sealing. Powder Technol. 154, 73–82.

Loulou, P., 1996. Direct numerical simulation of incompressible pipe flow using a B-spline spectral method. Ph.D. Thesis, Stanford University, Department of Aeronautics and Astronautics.

Mackrodt, P.-A., 1976. Stability of Hagen–Poiseuille flow with superimposed rigid rotation. J. Fluid Mech. 73, 153–164.

Markatos, N.C., 1986. Modelling of two-phase ftransient flow and combuston of granular propellants. Int. J. Multiphase Flow 12, 913–933.

Maxey, M.R., Riley, J.J., 1983. Equation of motion for a small rigid sphere in a nonuniform flow. Phys. Fluids 26, 883–889.

Mondt, E., Van Kemenade, H.P., Brouwers, J.J.H., Bramer, E.A., 2004. Rotating Sorbent Reactor. In: Celata, G.P., Di Marco, P., Mariani, A., Shah, R.K. (Eds.), third International Symposium on Two Phase Flow Modelling and Experimentation, Pisa, Italy.

Mondt, E., Van Kemenade, H.P., Schook, R., 2006. Operating performance of a naturally driven rotational particle separator. Chem. Eng. Technol. 29, 275–383.

Orlandi, P., Fatica, M., 1997. Direct simulations of turbulent flow in a pipe rotating about its axis. J. Fluid Mech. 343, 43–72.

Reeks, M.W., 1983. The transport of discrete particles in inhomogeneous turbulence. J. Aerosol Sci. 14, 729–739.

Sanmiguel-Rojas, E., Fernandez-Feria, R., 2005. Nonlinear waves in the pressure driven flow in a finite rotating pipe. Phys. Fluids 17, 014104.

Schlichting, H., 1979. Boundary Layer Theory. McGraw-Hill.

Van Kemenade, H.P., Mondt, E., Hendriks, A.J.A.M., Verbeek, P.H.J., 2003. Liquid phase separation with the rotational particle separator. Chem. Eng. Technol. 26, 1176–1183.

Van Wissen, R.J.E., 2006. Centrifugal separation for cleaning well gas streams: from concept to prototype. Ph.D. Thesis, Technische Universiteit Eindhoven.

Veenman, M.P.B., 2004. Statistical analysis of turbulent pipe flow: a numerical approach. Ph.D. Thesis, Technische Universiteit Eindhoven.

Wagner, C., Hüttl, T.J., Friedrich, R., 2001. Low-Reynolds number effects derived from direct numerical simulations of turbulent pipe flow. Comput. Fluids 30, 581–590.

Walpot, R.J.E., Kuerten, J.G.M., Van der Geld, C.W.M., 2006. Experimental determination of Lagrangian velocity statistics in turbulent pipe flow. Flow Turbul. Combust. 76, 163–175.

Westerweel, J., Draad, A.A., Van der Hoeven, J.G.Th., Van Oord, J., 1996. Measurement of fully-developed turbulent pipe flow with digital particle image velocimetry. Exp. Fluids 20, 165–177.

Yeung, P.K., Pope, S.B., 1988. An algorithm for tracking fluid particles in numerical simulation of homogeneous turbulence. J. Comp. Phys. 79, 373–416.